

AEDC-TR-80-39

C.2

B



## Program for Automated Holographic Data Reduction

R. W. Menzel and L. D. Vandergriff  
ARO, Inc.

August 1981

Final Report for Period October 1, 1979 – June 30, 1980

Approved for public release; distribution unlimited.

**ARNOLD ENGINEERING DEVELOPMENT CENTER  
ARNOLD AIR FORCE STATION, TENNESSEE  
AIR FORCE SYSTEMS COMMAND  
UNITED STATES AIR FORCE**

**UNCLASSIFIED**

## PREFACE

The work reported herein was conducted by the Arnold Engineering Development Center (AEDC), Air Force Systems Command (AFSC). The results were obtained by ARO, Inc., AEDC Group (a Sverdrup Corporation Company), operating contractor for the AEDC, AFSC, Arnold Air Force Station, Tennessee, under ARO Project Number P32L-02. Mr. Marshall K. Kingery was the Air Force project manager. The manuscript was submitted for publication on August 8, 1980.

Dr. R. W. Menzel is currently employed by Calspan Field Services, Inc., AEDC Division. Ms. L. D. Vandergriff is currently employed by General Research Corp., Fort Walton Beach, FL.

## CONTENTS

	<u>Page</u>
1.0 INTRODUCTION .....	5
2.0 CHARACTERISTICS OF HOLOGRAPHIC IMAGES .....	6
3.0 DESCRIPTION OF THE QUANTIMET IMAGE ANALYZING COMPUTER .....	8
4.0 HOLOGRAPHIC FEATURE DETECTION PROGRAM	
4.1 Program Outline .....	9
4.2 Detection Level Setting .....	10
4.3 Traverse Movement .....	11
4.4 Data Handling .....	11
5.0 IMAGE FOCAL PLANE DETERMINATION	
5.1 Detection Level Requirements .....	12
5.2 Focal Plane Detection Algorithms .....	13
5.3 Experimental Results .....	14
6.0 SUMMARY .....	16
REFERENCES .....	17

## ILLUSTRATIONS

Figure

1. Holographic Recording and Reconstruction Geometry .....	19
2. Ring Structure within the Reconstructed Particle Images .....	20
3. Intensity Profiles of a Particle Image as a Function of Out-of-Focus Distance .....	21
4. Block Diagram of the Quantimet Image Analyzing Computer .....	22
5. Detection Parameters Available with the MS3 Analyzer .....	23
6. Quantimet Evaluation of High-Contrast Microscopic Image of Wear Particles Immersed within Ambrex 43C Oil .....	24
7. Flow Chart of the Holographic Image Data Reduction Program .....	25
8. Detection Level Criterion .....	26
9. Flow Chart of the Detection Level Selection Program .....	27
10. Flow Chart of the Traverse Movement .....	28
11. In-Focus Reconstructed Particle Images as Observed at Different Detection Levels .....	29

<u>Figure</u>	<u>Page</u>
12. Detected Intensity Levels within Reconstructed Particle Images for Out-of-Focus Distance $\Delta z$ .....	30
13. Principle of the Area Difference Detection Algorithm .....	31
14. Flow Chart of the Focal Detection Algorithms .....	32
15. Focal Detection of a Particle Image Using the Detection Algorithms .....	33
16. Focal Detection by Area Difference of Holographic Particle Images .....	34
17. Focal Detection by Slice Mode Area of Holographic Particle Images .....	35
18. Focal Detection by Slice Area Divided by the Perimeter of Holographic Particle Images .....	36
19. Slice Mode Detection of Reconstructed Particle Images for Out-of-Focus Distance $\Delta z$ .....	37
20. Focal Detection by Mean Radius of Holographic Particle Images .....	38

## 1.0 INTRODUCTION

The wind tunnels and engine test cells at Arnold Engineering Development Center (AEDC) routinely use solid particle and liquid droplet fields to simulate desired atmospheric conditions in operational performance and material reliability tests of various aerodynamic systems. Holography has proved to be a viable technique for calibrating and analyzing the various kinds of particle and droplet fields (Refs. 1 through 5). The principal advantage of holography is that it allows an after-the-fact study of a three-dimensional field of interest. In particles fields the size, shape, number density, spatial distribution, and velocity can be extracted from the reconstructed images.

Although holography is an excellent calibration tool for particle field studies, its principal detriment is the considerable amount of time and operator attention necessary to make these measurements. For example, in the investigation of the subscale icing facility (RID) of the Engine Test Facility (ETF), approximately 18,000 particle images from 71 holograms were measured. The operator time required was about 850 hours. Aside from the extreme tedium of such a job, natural operator fatigue progressively sets in after a few hours, and images can be misinterpreted or missed entirely.

To reduce data reduction time and operator tedium and to improve of the accuracy and repeatability of the data, an automated data reduction program was initiated at AEDC. The design criteria were, in broad outline, similar to work by Bexon (Ref. 6). The criteria included the capability for image analysis versatility, and the ability of direct interface with a minicomputer. An existing Quantimet® system was modified to provide the system to perform the automatic readout function.

The central problem in automating the data reduction from holographic reconstructions is finding the focal locations of the images. This problem has two interdependent parts, the determination of the image detection levels, and finding a suitable focal detection algorithm. This report presents the progress, to date, in a continuing effort to construct an automated program for detecting and measuring holographically reconstructed images of particle fields. The physical principle for this technique is outlined in Section 2.0 where an analytical description of holographic image characteristics is presented. Section 3.0 briefly describes the Quantimet Image Analyzing Computer, and Section 4.0 outlines, with the aid of flow charts, the holographic image feature detection program. Section 5.0 discusses the image focal plane detection problem and the various detection algorithms that have been investigated. Finally, Section 6.0 summarizes and discusses the experimental requirements for the next phase of this work.

## 2.0 CHARACTERISTICS OF HOLOGRAPHIC IMAGES

The principal equation determining the characteristics of the reconstructed image of a circular particle for both the in-line and off-axis case is given by (Ref. 7)

$$A = 2a \int_0^R \exp \left\{ \frac{i}{2} \left( \frac{k_i}{z_i} - \frac{k_o}{z_o} \right) r^2 \right\} J_0 \left( \frac{k_i r_i r}{z_i} \right) J_1 \left( \frac{k_o a r}{z_o} \right) dr \quad (1)$$

where

$A$  = image amplitude

$a$  = particle radius

$k$  =  $2\pi/\lambda$

$\lambda_i$  = reconstruction wavelength

$\lambda_o$  = recording wavelength

$R$  = radius of the recorded holographic area

$J_n$  = Bessel function of the  $n$ th order

The geometrical parameters  $r$ ,  $r_i$ ,  $z_o$ , and  $z_i$  are shown in Fig. 1, which illustrates the off-axis case. The in-line case results for  $\alpha_o = \alpha_r = \alpha_i \equiv 0$ . Equation (1) has a closed form solution only for some special cases. For example, when the in-focus condition [ $(k_i/z_i) - (k_o/z_o) = 0$ ] is met, the maxima of the variation in the intensity distribution ( $I = AA^*$ ) within the particle image is obtained from

$$\left. \frac{dI}{dR} \right|_{\text{in focus}} = 2A \frac{dA}{dR} = 0 \quad (2)$$

where

$$\frac{dA}{dR} = \frac{2a}{R} J_0 \left( \frac{k_i r_i R}{z_i} \right) J_1 \left( \frac{k_o a R}{z_o} \right) \quad (3)$$

The radial locations ( $r_i$ ) of the extreme are determined by the  $J_0$  zeros. The number of intensity extrema for any given set  $k_o$ ,  $a$ ,  $z_o$ , and  $R$  is given by the number of  $J_0$  zeros contained within  $0 \leq r_i \leq a$ . Thus, the image intensity is not a constant within the particle radius, but rather the intensity profile is similar to a series of concentric rings. This condition is true also as the image goes out-of-focus with the additional feature that the intensity variations become more pronounced, as is shown in Fig. 2. The importance of the ring structure is that it complicates choosing an intensity threshold by which the presence of an image may be detected.

Equation (1) may be wrestled into an approximated closed form solution for the out-of-focus condition  $(k_i/z) - (k_o/z_o) \cong \delta z$   $k_o/z_o^2$  ( $\delta z$  being small) at the edge of the image ( $r_i = a$ ). The intensity is

$$I|_{r_i=a} \cong \left( \frac{z_o}{k} \right) \left\{ \left[ 1 - J_o^2(x) \right] - \frac{\delta z}{z_o} x^2 \left[ J_1^2(x) - J_o(x) J_2(x) \right] \right\}^2 \quad (4)$$

where  $x = k_o a / R/z_o$ . From this, the slope at the geometrical particle edge within the image is obtained

$$\begin{aligned} \frac{dI}{dr_3} \Big|_{r_i=a} &\cong 2R^2 \left\{ \left( 1 - J_o^2(x) \right) \left( J_1^2(x) - J_o(x) J_2(x) \right) - \frac{\delta z}{z_o} \left[ x^2 \left( J_1^2(x) - J_o(x) J_2(x) \right)^2 \right. \right. \\ &\quad \left. \left. - J_1^2(x) \left( 1 - J_o^2(x) \right) \right] \right\} \end{aligned} \quad (5)$$

The slope decreases with an increasing out-of-focus value  $\delta z$ , and the in-focus location of the particle image may be determined from the maximum slope near the image edge.

This point is further illustrated in Fig. 3, which shows the intensity profile across one-half of a particle image at various positions on either side of the focal plane. Clearly, the slope near the edge of the image decreases as the out-of-focus distance increases. Similarly, the image perimeter decreases with increasing out-of-focus distance. The intensity variations within the image and the increase of these variations with increasing out-of-focus distance is also observable.

Equation (4) provides an estimate of the out-of-focus step size that causes a perceptible change in the image appearance. The criterion for perceptible change is taken from the usual definition of focal length (Ref. 8) in which a somewhat arbitrary 20-percent reduction in intensity of the focal spot is permitted either side of the actual focal plane. Applying this to the intensity at the edge ( $r_i = a$ ) of the image, the approximation

$$\delta z \frac{x^2}{z_o} \left[ J_1^2(x) - J_o(x) J_2(x) \right] \approx 0.2 \quad (6)$$

mimics the focal depth definition. Using the asymptotic approximation for the Bessel function, the expression may be simplified to

$$\delta z \approx 0.2 \frac{\pi z_o}{2} \left( \frac{z_o}{k_o a R} \right) \quad (7)$$

This equation provides an estimate of the step size to be used in the traverse system when it searches for the focal plane.

The signal-to-noise ratio of the reconstruction images is due partly to film characteristics (Ref. 9) and to speckle phenomena (Ref. 10). Decreased film grain sizes cause smaller speckle sizes, and improved emulsion development techniques increase the diffraction efficiency of the hologram (Ref. 11). The statistics of the speckle phenomena require that some speckle spots have a maximum intensity. This is important when the problems of image detection are considered, because some speckle noise that cannot be filtered from the desired particle images by proper intensity threshold settings will always reside within the reconstructed image field. Examples of experimental image intensity profiles for in-line holography show that often the signal-to-noise ratios of good holographic reconstructed images are no better than about two (Refs. 11 and 12). Off-axis holography is better, in principle, because the image is physically separated from the reconstruction illumination and the out-of-focus conjugate image. However, the improvement is often experimentally ineffective because of unavoidable noise in the recording illumination. An example is the phase front distortion caused by turbulence in the medium entraining the particle field. In the reconstruction the turbulence contributes background intensity variations similar to large scale speckle.

### **3.0 DESCRIPTION OF THE QUANTIMET IMAGE ANALYZING COMPUTER**

The Quantimet 720 Image Analyzing Computer (Cambridge Instrument Co., Inc.), is a system of modules hardwired together to measure features within a high-contrast optical image. Figure 4 is a block diagram of the main system components.

The image to be studied is focused onto the Vidicon Detector, a high-resolution system of 720 raster scans. Each scan line is resolved into 910 picture points of fixed size and location. All measurements are made from the intensity level within each of the approximately 650,000 picture points. The System Control of the Vidicon (Cambridge IMANCO technical data sheet 7213/I) provides control of the scan and video processing, timing, pulse generation, and character generation (alphanumerics) for the visual display. The Display Unit (data sheet 7214) converts the signals for a visual display and highlights on the visual display unit those picture points that satisfy the desired intensity profile.

The ID Auto Detector (data sheet 7221/1A) selects the features in the field-of-view to be measured according to an intensity gray scale of 64 steps. Three detection criteria are available: (1) intensities less than a selected level, (2) intensities greater than a selected level, and (3) intensities falling between two selected levels, the so-called slice mode. Computer control of the detection level and mode setting is available. A Light Pen Module (data sheet 7229) allows the operator to select specific images within the field-of-view on the video display monitor for detection and measurement.

When image detection is completed, the picture points are processed by the Standard and Function Computers (data sheet 7221/1 and 2). The Standard Computer MS3 Analyzer provides area, intercept, perimeter, and count measurements. In addition, by proper size selection, small features (i.e., noise) may be removed from these measurements. These four basic measurements are used by the Function Computer to deduce the additional feature measurements listed in Fig. 5. This module may be addressed by the DEC PDP-11 computer.

The Computer Data Interface (Field, Image, Feature Interface, data sheet 7249) allows data storage in a DEC PDP-11 computer system and also displays alphanumerical commands from the computer on the visual monitor. Computer control of the 1D Auto Detector is provided by the Control Interface (data sheet 7241).

It is difficult to exaggerate the versatility of the Quantimet system for analyzing high-contrast image fields, particularly when incoherent illumination is used and the problematic interferometric noise of coherent illumination is avoided. For example, the Technical Support Department Chemistry Laboratory at AEDC routinely uses the Quantimet to count and size wear particles immersed in oil. The particles are separated from the oil by drawing oil samples through filter paper. A microscopic image of the resulting particle field is focused onto the Vidicon Detector. The Quantimet counts, sizes, and stores in histograms as many fields-of-view as are desired. Figure 6 shows both the video display for a typical sample and a histogram from multiple sample fields. The time required to perform this operation is little more than the microscope set-up time. In contrast with manual counting and sizing, a considerable advantage is gained in both the number of samples being investigated and the repeatability of the results.

## 4.0 HOLOGRAPHIC FEATURE DETECTION PROGRAM

### 4.1 Program Outline

The procedural steps necessary to reduce data from holograms using the Quantimet system are in broad outline as follows:

1. The hologram is reconstructed while mounted in an (x,y,z) traverse system. The traverse system allows the positioning of various focal planes onto the fixed Vidicon Detector.
2. The traverse system is set to its initial position.
3. The image field is investigated and all potential particle image positions are stored.

4. The traverse moves in incremental z distances and the image field is repeatedly investigated.
5. An algorithm is continuously applied to determine the focal plane locations of the particle images.
6. At the end of a completed z movement, the traverse moves an incremental x or y step to a new field-of-view and the computer-controlled procedure repeats itself.

The DEC PDP-11 basic program for holographic image feature detection has four main functional sections: detection level setting, computer-controlled traverse movement, focal plane detection and image measurement, and data storage. The general flow chart for the program is shown in Fig. 7.

#### **4.2 Detection Level Setting**

As shown in the flow chart in Fig. 7, there are three choices for the detection level setting. The manual mode allows the operator to select the detection level. The Quantimet provides feedback to the operator by showing identifying marks called anti-coincident points (ACP's) on the video display for all detected features. This also allows the operator to search for the detection range that is most sensitive to image features while still rejecting background noise. Experimentally, the effective range for detecting holographically reconstructed images is only about 6 to 7 levels out of the 64 available; above this range, images are not detected, while below too much noise is detected. Subsequently, all image characteristics can be resolved no better than these 6 to 7 gray levels.

As an aid to finding the useful range of the detection levels, a semi-automatic mode may be used. The algorithm for determining this may be understood with the aid of Fig. 8. Consider the hypothetical case where the image field contains a single feature that has a square wave intensity profile (Fig. 8a). A plot of the area measured as the detection level steps successively through L1, L2, etc., exhibits a plateau for a given range of the detection levels (Fig. 8b). Below the plateau region, noise contributes to the detected area. In principle the plateau region defines the useful detection level range. For a real particle image (Fig. 8c) the field area detected (Fig. 8d) has a less well-defined plateau, but the principle can still be applied. For multiple image fields-of-view and/or for low-contrast images, the plateau region length decreases further and the detection level must be judgmentally chosen from the slope at the detected field area curve.

Figure 9 gives a more detailed flow chart of the detection level settings. The field detection area is displayed in histogram form from which the operator deduces the detection

level settings and manually enters them into the program. The fully automatic detection selection portion of the program remains to be written because determination of the threshold levels from the field detection area curve needs further study. Experimentation shows that each particle image generates a somewhat different curve; consequently, generalized detection level requirements have not yet been successfully defined.

#### 4.3 Traverse Movement

The traverse movement of the holographic film holder is designed to allow determination of the focal location of each particle image within the three-dimensional reconstruction field. The hologram is moved so that a different region of the reconstructed field may be presented to the fixed focal plane of the stationary Vidicon Detector.

Figure 10 shows the flow chart of the computer-controlled  $(x, y, z)$  traverse motion. Initial conditions are determined from the experimental conditions during the holographic recording and are manually entered into the program. The step sizes are obtained from Eq. (7) for  $\delta z$ , and from the Vidicon field of view for  $\Delta x$  and  $\Delta y$ . All three step sizes must be corrected for the magnification of the Vidicon Detector optics. Thus, the  $\delta z$  step given by Eq. (7) must be multiplied by the lateral magnification squared to obtain  $\Delta z$ . The number of steps necessary for a complete traverse are again determined from the recording conditions and are manually entered into the program.

Beginning at location  $(0,0,0)$  the traverse steps  $n$  times through  $\Delta z$  until  $(0,0,z_{\max})$  is reached. A  $\Delta x$  step is executed and  $\Delta z$  is made negative. The traverse movement travels in the opposite  $z$  direction until  $(\Delta x, 0, 0)$  is reached, at which point another  $\Delta x$  step and  $\Delta z$  sign reversal is made. This continues until  $x_{\max}$  is reached, where a  $\Delta y$  step is executed and  $\Delta x$  and  $\Delta z$  are changed in sign. The entire image space has been traversed when  $y_{\max}$  is reached.

#### 4.4 Data Handling

For each step, all images exceeding the detection level are measured and stored according to their  $(x, y, z)$  location. Not all images are, of course, in focus and much of the data must ultimately be rejected. Data from multiple  $\Delta z$  steps are compared to find the focal location of each image. In effect, a history of the image characteristics that is used as the input to a focal detection algorithm is formed as it moves in the  $z$  direction. Subsequent to detection, only the focal-plane information is retained.

Another data handling problem is that the  $(x, y)$  coordinates for an image do not remain stationary as  $z$  moves. This is a combined effect of optical bench vibration and changes in

the image shape and intensity characteristics which are  $z$  dependent. Images are therefore defined to be the same when the  $(x,y)$  coordinates for successive  $\Delta z$  positions fall within a tolerance circle. Experimentally, the tolerance circle has a radius of about 20 picture points. The effect of the tolerance circle on the data is to limit the size resolution of the acceptable images and/or their spatial density. Both size and spatial density can generally be brought into acceptable tolerance by an adjustment of the viewing optics magnification.

## 5.0 IMAGE FOCAL PLANE DETERMINATION

### 5.1 Detection Level Requirements

The most critical section of an automated program for obtaining data from reconstructed particle images is finding the focal location of each image. When images are visually observed the operator makes simultaneous judgments on image clarity, watching a set of diffraction rings collapse to the image edge as it comes into focus, and observing the general uniformity of the image illumination. These processes can be physically described. Clarity corresponds to the intensity slope near the edge of an image or for any abrupt transition in the image. Generally this also implies larger intensity transitions. The collapsing diffraction ring is a moving intensity pattern that relates concentrically to the image location. Whereas the observer's eye can easily recognize the spatial pattern and integrate the motion to infer focal position, the process also requires rejecting information which is not germane to the image. In a machine which regards all signals with equal weight, noise rejection is difficult to perform. Judging the overall uniformity of an image requires a continuous adjustment of the mean sensitivity level and finding the position which corresponds to a least deviation about the mean. This necessitates an intensity level value being attached to each picture point, something for which the Quantimet is not set up.

The Quantimet is, in fact, prepared for only one type of detection: intensity comparison with a fixed, gray scale. Feature selection and measurement results from a subsequent grouping of adjacent picture points that meet the selected gray scale requirements. Should an interruption in the continuity of "adjacency" exist, the Quantimet's detection logic regards these as though separate features are present. This feature makes intensity level settings particularly critical for reconstructed images because the detection level must be set lower than the normally occurring intensity dips within the image.

Figure 11 illustrates this point. The intensity threshold level is too high in Fig. 11a so that no image is adequately recognized. As the level is lowered, the smaller images are detected fully, but the larger images are still inadequately detected. When the level is further lowered to allow complete detection of the larger images, noise in the background has become a

significant part of the overall detected features. The sensitivity of the Quantimet to detection level setting is also illustrated in that all the images in Fig. 11 were to an observer's eye equally intense before the detected areas were highlighted.

Relevant to Fig. 11, all the holographic images in this report are the in-line reconstructions of a microscope reticle. The recording was on Agfa Gaevert® 8E75 film and was developed to a density of about 0.8 to 1.0 by normal D-19 development. The recording and reconstruction illumination were plane waves of  $\lambda = 0.6328 \mu\text{m}$  and 10 cm diameter, and the reconstruction distance was 7 cm. All the images are white features detected against a darker field.

The effect of a single choice for the detection level on the detected area of out-of-focus images is shown in Fig. 12. The ring structures within the image becomes quite pronounced, with an increasing effect for increasing  $\Delta z$ . Some of the images are clearly displayed as separated detection areas.

## 5.2 Focal Plane Detection Algorithms

Equation (5) shows that the slope of the intensity of the image edge is maximum when the image is in focus. Since slope detection is not directly available an approximation is made, as illustrated in Fig. 13. Two levels of detection are set such that one is just above the background noise and the other is somewhat below the intensity at which the ring structure in the image is detected. Area readings are made at each of the detection levels. The difference in the areas is proportional to slope and is at a minimum when the image is in focus. In the procedure for finding the focal plane, the area difference is monitored at each  $z$  location and the focal location is considered to occur where the area difference is at a minimum. This proceeds simultaneously for all the potential particle images at each  $z$  location.

Several studies of automated holographic data reduction using a Quantimet system have been made. Trolinger (Ref. 13) proposed detecting the images using the slice mode such that only the area of the image between two detection levels is measured. The two detection levels are adjacent gray levels that lie half-way between the background noise and the maximum intensity across the reconstructed image. Trolinger found that the slice mode area is minimized as the image is focused.

The distinction between the slice mode area and the area difference at two levels arises from the Quantimax operation. In the area difference method the two area measurements are made even though the areas may be imperfectly detected. On the other hand, the slice

mode detection of images which lack uniform intensity distribution can result in the slice being detected in discontinuous portions, each of which the Quantimet considers as a separate image. Thus, the convenience of the slice mode detection is often offset by erroneous data generation.

Bexon (Ref. 14) alleviates the slice mode problem by incorporating a 2D Amender unit into his Quantimet system. The Amender allows controlled modifications to be made to the detected video signals. An image may be "filled in" to compensate for low intensity spots within the image. Bexon's method of focal plane detection requires measurement of the slice mode area and the perimeter of the slice. The ratio of the area to the perimeter ( $A/P$ ) is required to fall within limits  $x < A/P < y$  "where  $x$  and  $y$  can be set on a standard recognition module. . ." Furthermore, "a scheme which is specific to each particle and does not rely on absolute  $x$  and  $y$  values has been devised by using the on-line Hewlett-Packard 9830<sup>®</sup> computer and CFFI module." For the examples shown (Ref. 14),  $A/P$  is minimized when the image is in focus. Bexon also finds that the mean radius (defined as the difference of the inner and outer diameters of the cross section at the slice mode, divided by two) has a minimum value at focus. The diameters are actually computationally derived from the area measurements.

Figure 14 is a flow chart of the focal plane detection algorithms. All the methods described have been incorporated into the flow chart, including a search program for a curve pattern which is discussed in Section 5.3.

### 5.3 Experimental Results

Several comments apply to the experimental results within the report. First, the reconstructed images were inline reconstructions of a microscope reticle. The holograms were made as already described and projected high-quality images in the reconstructions. The in-focus images are shown in Fig. 11. Second, the graphs in the figures each demonstrate a focal location algorithm and, as such, were generated by a program apart from the holographic data reduction program. Third, all measurements made with the Quantimet were repeated at least ten times to allow for the influence of system noise. The noise was caused partly by an intractable grounding problem and partly by a mechanical vibration of the optical bench. The vibration originated with the fan in the Vidicon housing and the stepping motors of the traverse system which are continuously "seeking" their locked-in position. Generally the noise caused a 2 percent to 3 percent deviation for any measurements of a stationary image.

To test the focusing algorithms apart from the holographic image-generating process, a 100- $\mu\text{m}$  circular particle was imaged on the Vidicon using coherent illumination. Figure 15 shows the area difference, the slice area/perimeter, and the mean radius versus the stepped z position relative to the focal location. Each z step is 12.5  $\mu\text{m}$ . The units for area, perimeter, and mean radius are all in picture points (p.p.) since that is the unit used by the Quantimet. This leads to the peculiarity that area divided by perimeter results in a dimensionless number. The error bars are representative and are similar in all cases. The focal location is clearly identifiable by the absolute minimum location on the curves. Several comments may be made. In none of the cases is the focal position a very sensitive function of the  $\Delta z$  change. Also, the numerical values serve as a best case guide for the subsequent holographic image detection curves. An increase in the numerical values in the latter case is a reflection of the noise that is part of the holographic image.

Figure 16 demonstrates the area difference algorithm for three holographically reconstructed particle images of different size. The detection levels used for all three images were chosen to best suit the image numbered 8 in Fig. 11. Focal detection within  $\Delta z \cong 250 \mu\text{m}$  is observed for images 8 and 10, whereas for the 12.5 image the algorithm failed. These results, which are typical of many measurements, demonstrate that for proper identification of every particle image, the detection levels must be selected for each image.

Figure 17 shows similar results for the slice mode area detection. The detection levels were chosen for image number 8. The 12.5 image case has such large error bars for two of the key points that the success of the algorithm is questionable. Figure 18 shows the area/perimeter detection which failed in all but the case for which the detection levels were chosen (image 15). The results of Figs. 17 and 18 demonstrate the difficulty of using the slice mode detection when the correction feature of the 2D Amender module is not available. This interpretation is emphasized by the slice mode detection images shown in Fig. 19. With the detection levels set for best results on the in-focus number 8 particle image, considerable noise in the form of non-peripheral area detection is present in all images. When the detection levels are raised to exclude interior area detection, the slice area is discontinuous. Consequently, the Quantimet gives measurement readings for many small area sections rather than for the total slice areas of the desired images. Incomplete detection because of intensity variations within the image is also the cause for the inadequate focal detection by the mean radius algorithm shown in Fig. 20. The detection levels in this case were adjusted for best detection on image 15.

An additional comment applies to the focal detection algorithm curves. In each case of successful detection of the focal plane shown in the figures, the curve has more than one point of zero slope. Thus, focal detection that is based on the encounter of a minimum

condition of the detection algorithm as the traverse scans through the z direction is not sufficient. It is necessary, rather, to generate the curve including points on both sides of focus and then extrapolate the focal location. An extrapolation which may be adequate but which needs further testing is to identify the focal plane with the location of the absolute minimum point on the curve.

## 6.0 SUMMARY

The problem of automated data reduction from holographic images of particle fields may be considered to consist of two parts. The first of these, the logistics of the hologram motion, feature measurement, and data storage, has been successfully completed and is incorporated into the holographic data reduction program. The logic of the program has been discussed and presented in flow charts.

The second part of the problem, which is finding the focal location of each particle image, has been addressed with partial success. The details of the image near focus have been theoretically derived and suggest that the most distinctive feature of a particle image coming into focus is the increasing slope near the edge of the image. This correlates with the increased image "sharpness" that is visually observed. Since the basic measurement of the Quantimet system is intensity difference detection, approximation techniques are necessary to measure the slope variable.

Three focal plane detection algorithms have been experimentally tested. Each was only partially successful which, in turn, led to the following conclusions on experimental requirements:

1. The Quantimet detection level settings are extremely critical and ideally must be individually set for each image;
2. Position, size, perimeter, and other data measured by the Quantimet must be multiply made and averaged. The standard deviations are typically sufficiently large that an individual measurement can lead to erroneous focal plane location;
3. Focal plane determination may have to be made from a curve-fitting program rather than from a simple minimum detection. This necessitates more extensive logic discrimination and data handling than is available from the progress in its present form;
4. As indicated by Bexon's results (Ref. 14), image discrepancies may be reduced with the addition of a 2D Amender module to the Quantimet system; and

5. High-quality reconstructed images are necessary because of the relatively restricted signal-to-noise range of holographic images and because of the restricted useful range of gray levels when viewing holographic images.

In the present form the detection algorithm has about a 50 percent chance of successfully finding the in-focus particle image. A considerably better detection rate is available when the program is reduced to a semi-automatic status. In this form all operations are computer controlled except that an operator determines the focal location of images and selects them for analysis with the light pen module. This type of program retains all the advantages of the Quantimet measuring capabilities and the computer data analysis, and because of these advantages, will still allow more rapid and accurate data reduction than by conventional means. Some holographic applications, particularly transilluminating fields of high turbulences, will require semi-automatic data reduction because the signal-to-noise ratio from those holograms precludes automated image identification. This is likely to remain so until the subtleties of the visual image and focus recognition are more precisely described in physical terms. Even then it is an open question if a machine such as the Quantimet, which only works on intensity difference detection, can be programmed to mimic those physical functions.

Improvements to the present image detection system can proceed along three directions. First, continued research is needed to improve the focal plane detection algorithms. Additional algorithms and/or a combination of detection requirements can probably increase the percentage of successful image detections. Second, the Quantimet system can be augmented with the Amender unit to allow more versatile algorithm programming. Third, improvements in the image source, the holographic process, need to be investigated. A potential candidate is the image cancellation technique (Ref. 15) applied to reducing the background radiation components in the reconstructed image field.

## REFERENCES

1. Farmer, W. M., Burgess, K. S. and Trolinger, J. D. "Holocamera for Examination of Water Droplet in a High Altitude Test Cell," AEDC-TR-70-181 (AD715916), December 1970.
2. Dougherty, N. S., Jr., and Belz, R. A. "In-Line Holography of Liquid Propellant Injection During Combustion," Proceedings Ninth JANNAF Combustion Meeting, CPIA Publication 231, Vol. 2, Monterey, California, September 11-15 1972, pp. 289-307.

3. Trolinger, J. D., and Belz, R. A. "Holography in Dust Erosion Tunnels," AEDC-TR-73-160 (AD766420), September 1973.
4. Lennert, A. E., et. al., "Electro-Optical Techniques for Diesel Research," AIAA Paper No. 76-78 Proceedings of the AIAA 14th Aerospace Science Meeting Washington, D.C., January 1976.
5. Belz, R. A., and Menzel, R. W. "Particle Field Holography at Arnold Engineering Development Center," *Optical Engineering*, Vol. 18, May — June 1979.
6. Bexon, R., Bishop, G. D. and Gibbs, J. "Aerosol Sizing by Holography Using the Quantimet," IMANCO Report on Equipment and Applications, No. 3.
7. Menzel, R. W., "Fundamental Properties of Holographically Reconstructed Images," PhD Dissertation in Physics, University of Tennessee, December 1975.
8. Born, M., and Wolf, E., *Principles of Optics*, Pergamon Press, Oxford, New York, 1975 (Fifth Edition).
9. Smith, H. M.,(ed.), *Holographic Recording Materials*, Springer-Veilag, New York, 1977.
10. Dainty, J. C., Editor, *Laser Speckle and Related Phenomena*, Springer-Verlag, New York, 1975.
11. Dunn, P., and Walls, J. M., "Absorption and Phase In-Line Holograms: a Comparison," *Applied Optics*, Vol. No. 13, 1979, pp. 2171-2174.
12. Belz, R. A., "An Investigation of the Real Image Reconstructed by an In-Line Fraunhofer Hologram Aperture-Limited by Film Effects," PhD Dissertation in EE, University of Tennessee, August 1971.
13. Trolinger, J. D., "Examination of Automatic Data Reduction Methods for Particle Field Holograms," Environmental Protection Agency Report EPA-600/2-79/005, January 1979.
14. Bexon, R., Gibbs, J. and Bishop, G. D., "Automatic Assessment of Aerosol Holograms," *J. Aerosol Sci.*, Vol. 7, 1976, pp. 397-407.
15. Trolinger, J. D., "Application of Generalized Phase Control During Reconstruction to Flow Visualization Holography," *Applied Optics*, Vol. 18, No. 6, 1979, pp. 766-774.

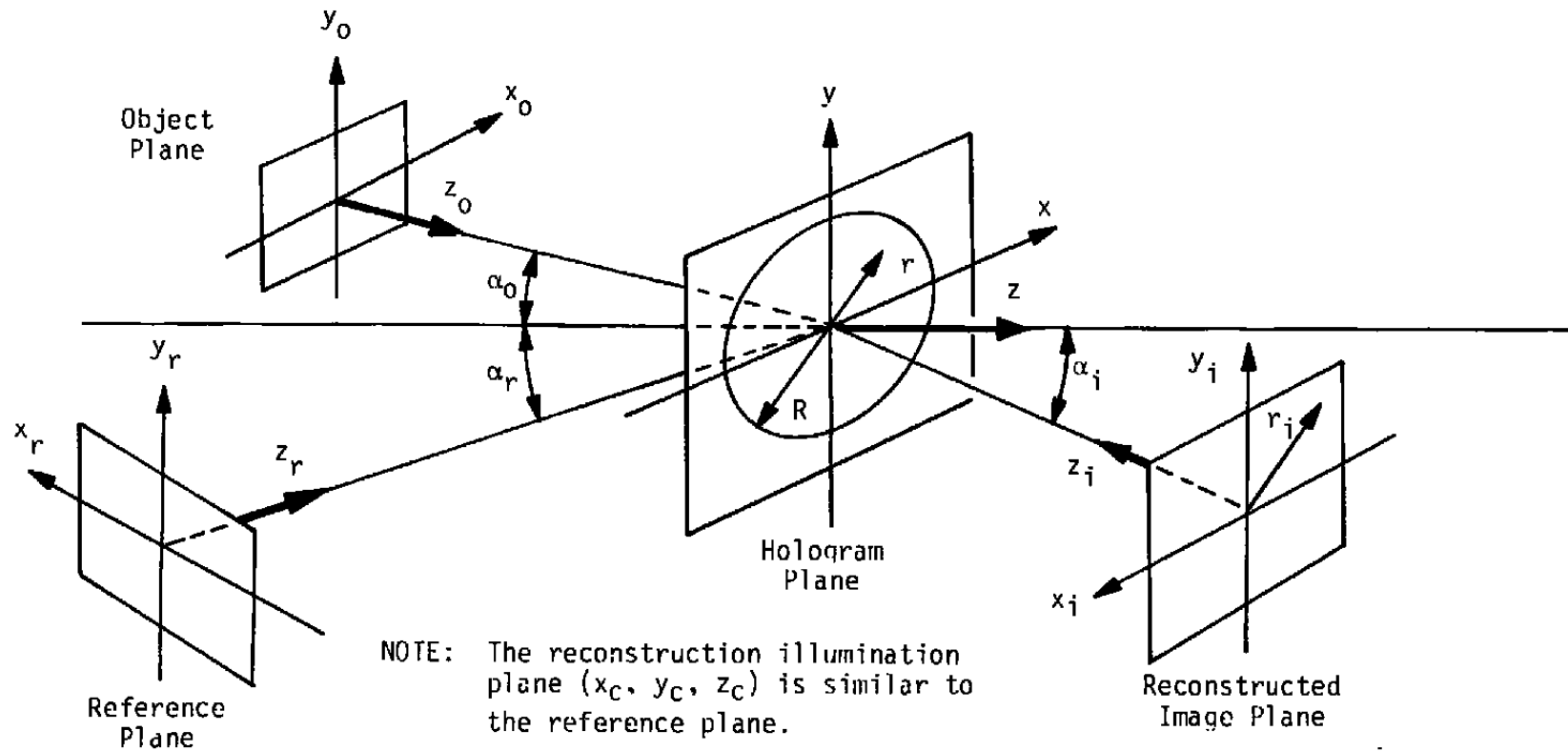
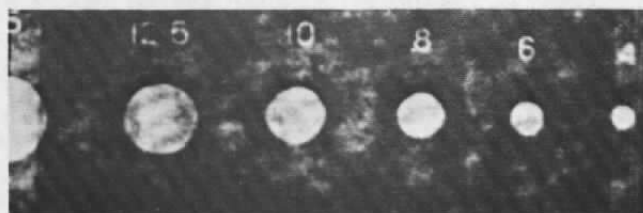


Figure 1. Holographic recording and reconstruction geometry.



a.  $\Delta z = 0$



b.  $\Delta z = 625 \mu\text{m}$



c.  $\Delta z = 1,250 \mu\text{m}$



d.  $\Delta z = 1,875 \mu\text{m}$



e.  $\Delta z = 2,500 \mu\text{m}$

Figure 2. Ring structure within the reconstructed particle images.

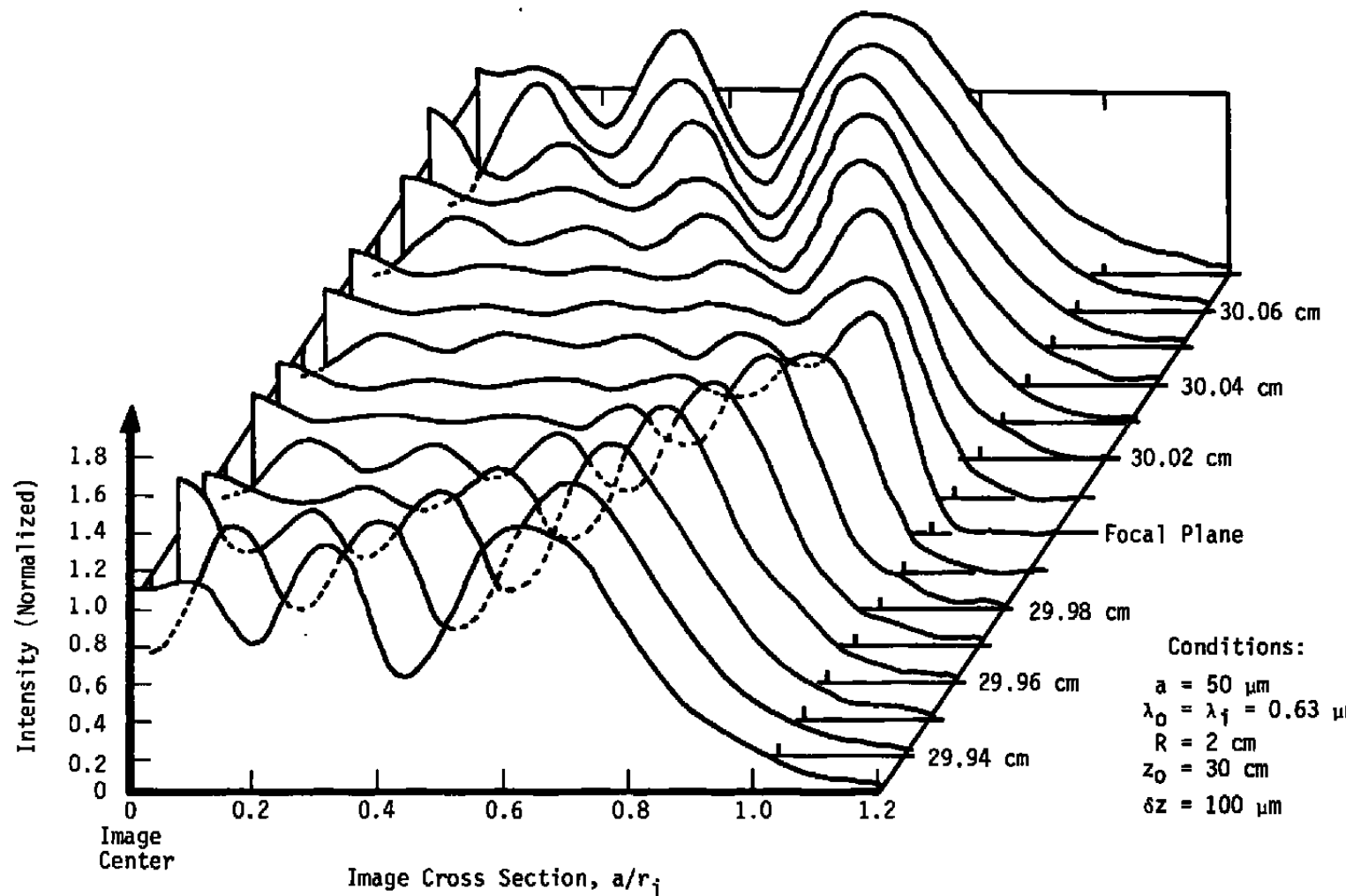


Figure 3. The intensity profiles of a particle image as a function of out-of-focus distance.

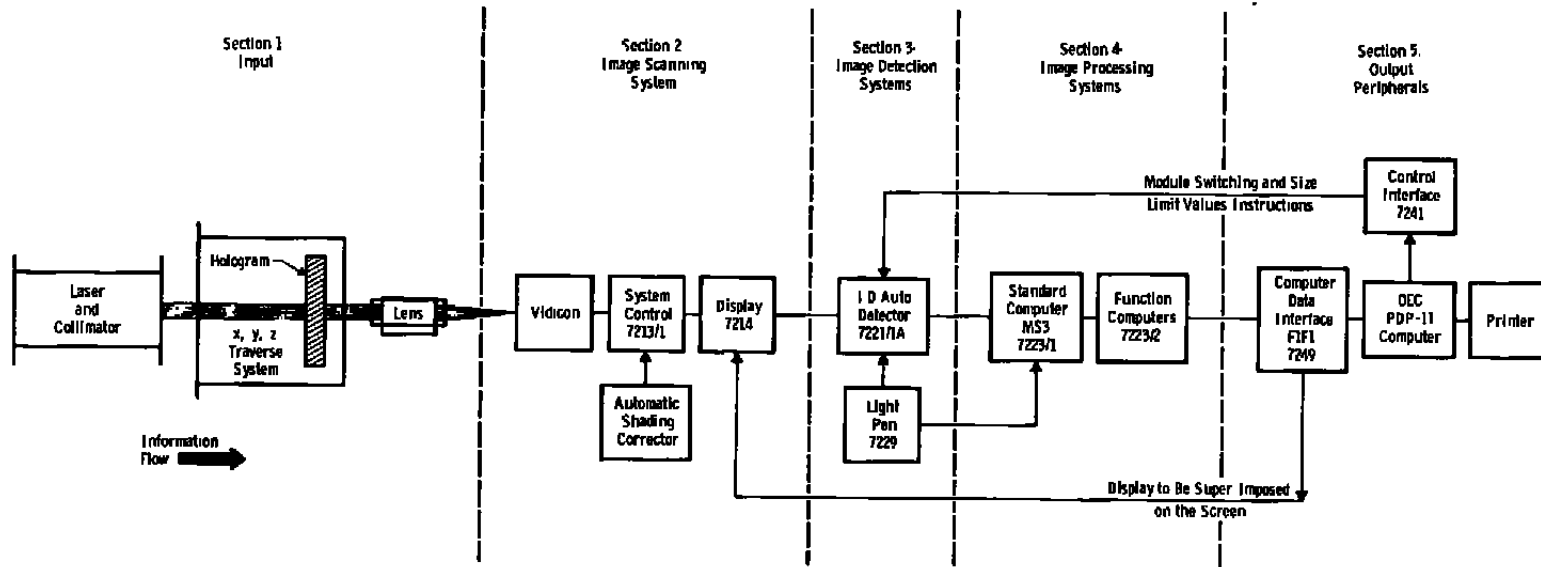


Figure 4. Block diagram of the Quantimet Image Analyzing Computer.

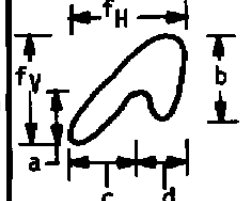
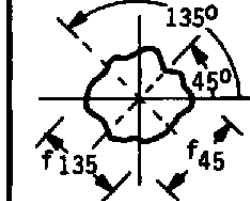
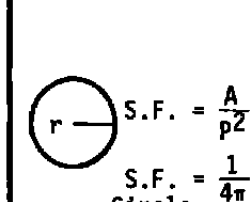
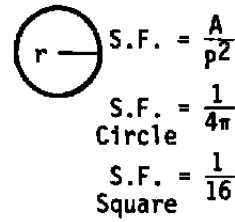
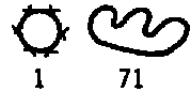
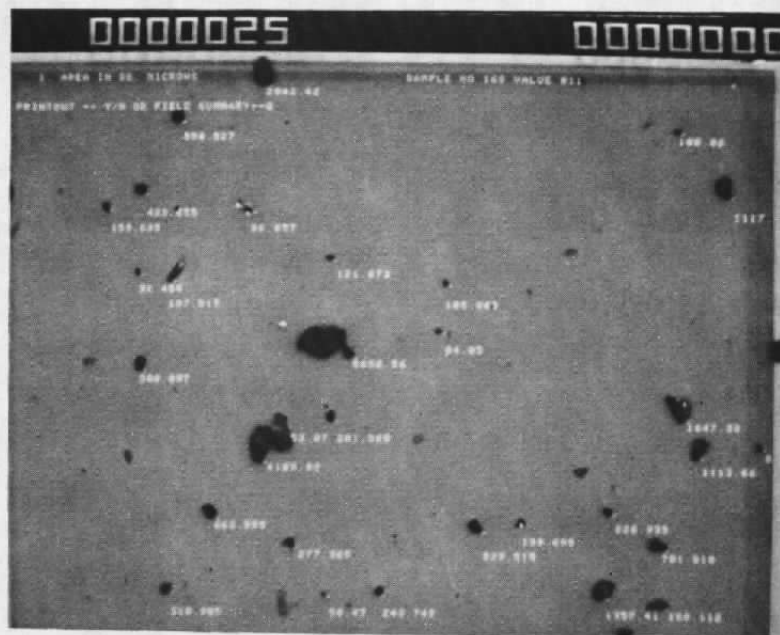
Parameter		Detected Feature
(A) Area	Size of the Particle	
(P) Perimeter		
( $H_p/V_p$ ) Horizontal & Vertical Projections	$H_p = a + b$ $V_p = c + d$	
( $f_H, f_V$ ) Horizontal & Vertical Ferets	Also Called "Caliper Diameters"	
( $f_{45^\circ}, f_{135^\circ}$ ) $45^\circ$ & $135^\circ$ Ferets	"Caliper Diameters" Coordinate Axis at $45^\circ$	
( $f_L, f_S$ ) Longest & Shortest Dimension	Longest & Shortest of $f_H, f_V, f_{45^\circ}, f_{135^\circ}$	
(S.F.) Shape Factor	An Indicator of Image Shape ( $A/P^2$ )	
<u>Convex Perimeter</u>	An Indicator of Image Complexity: $\frac{(\pi)}{4} \frac{(f_H + f_V + f_{45^\circ} + f_{135^\circ})}{P}$	
Perimeter	$\frac{C.P.}{P} \approx 1$ Circle	
Elongation Ratio	$(f_{\max}/f_{\min})$ Circle = 1	
(V) Volume		

Figure 5. Detection parameters available with the MS3 analyzer.



a. Video screen output with feature area superimposed

Summary to Date of Sample No. 16S Valve #11

Range, m	Number of Particles	Avg/Field	Total Particles
5 - 15	89	11.125	5,084.13
15 - 25	89	11.125	5,084.13
25 - 50	93	11.625	5,312.62
50 - 100	40	5	2,285
100 - 9,999	9	1.125	514.125

b. Computer printout of multiple field feature sizing

Figure 6. Quantimet evaluation of the high contrast microscopic image.

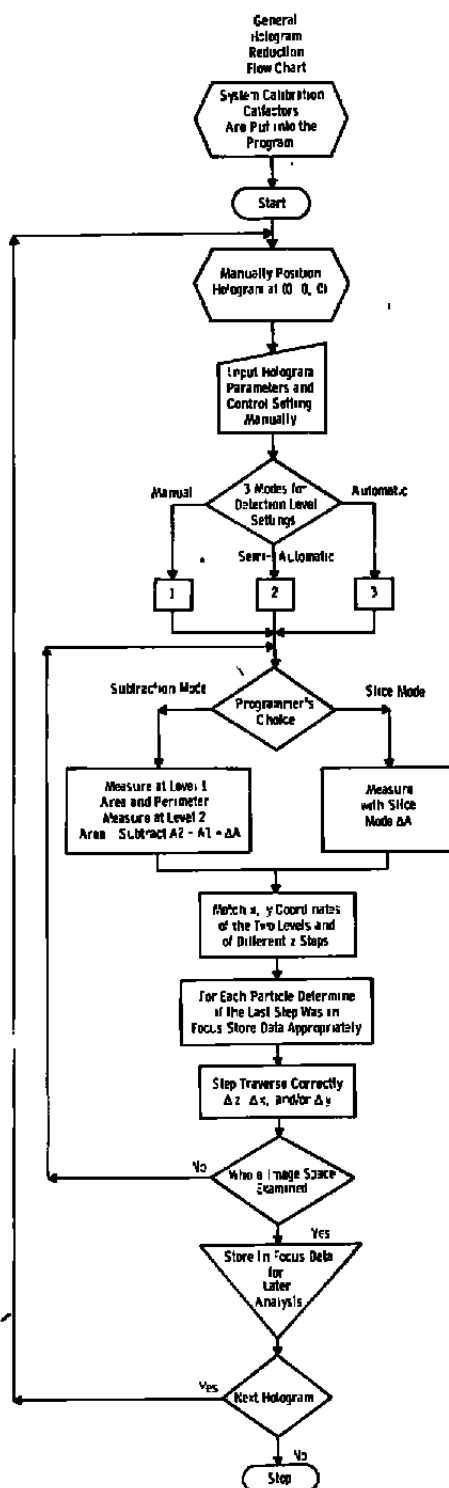


Figure 7. Flow chart of the holographic image data reduction program.

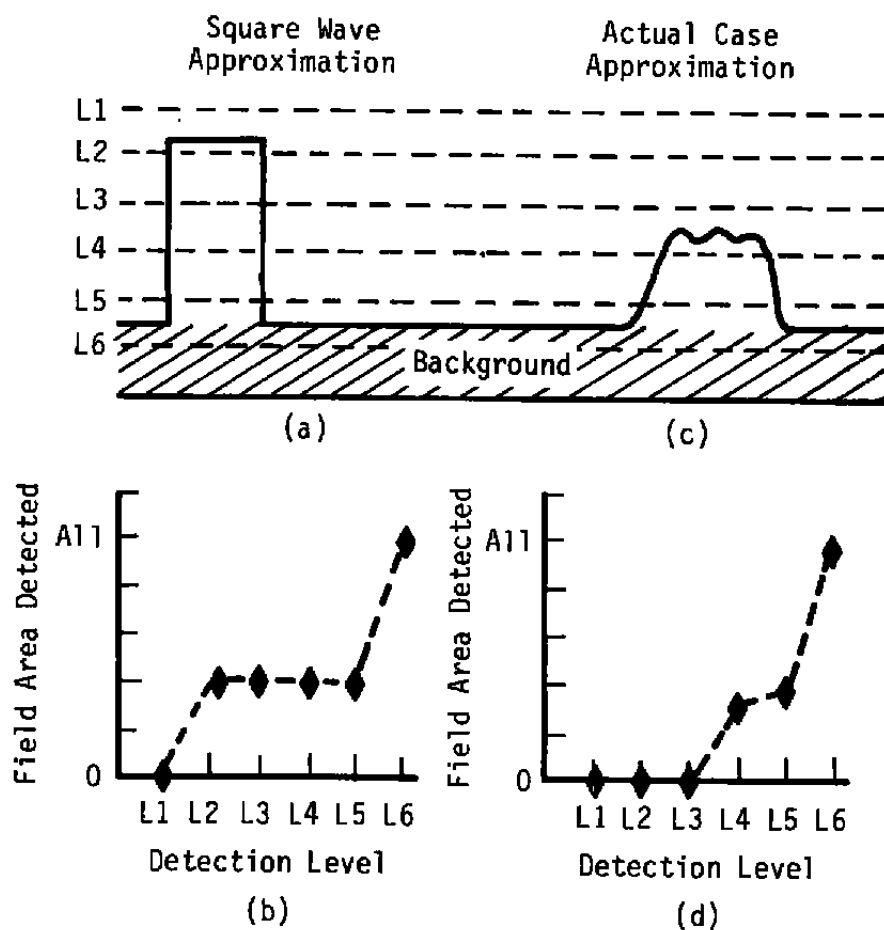


Figure 8. Detection level criterion.

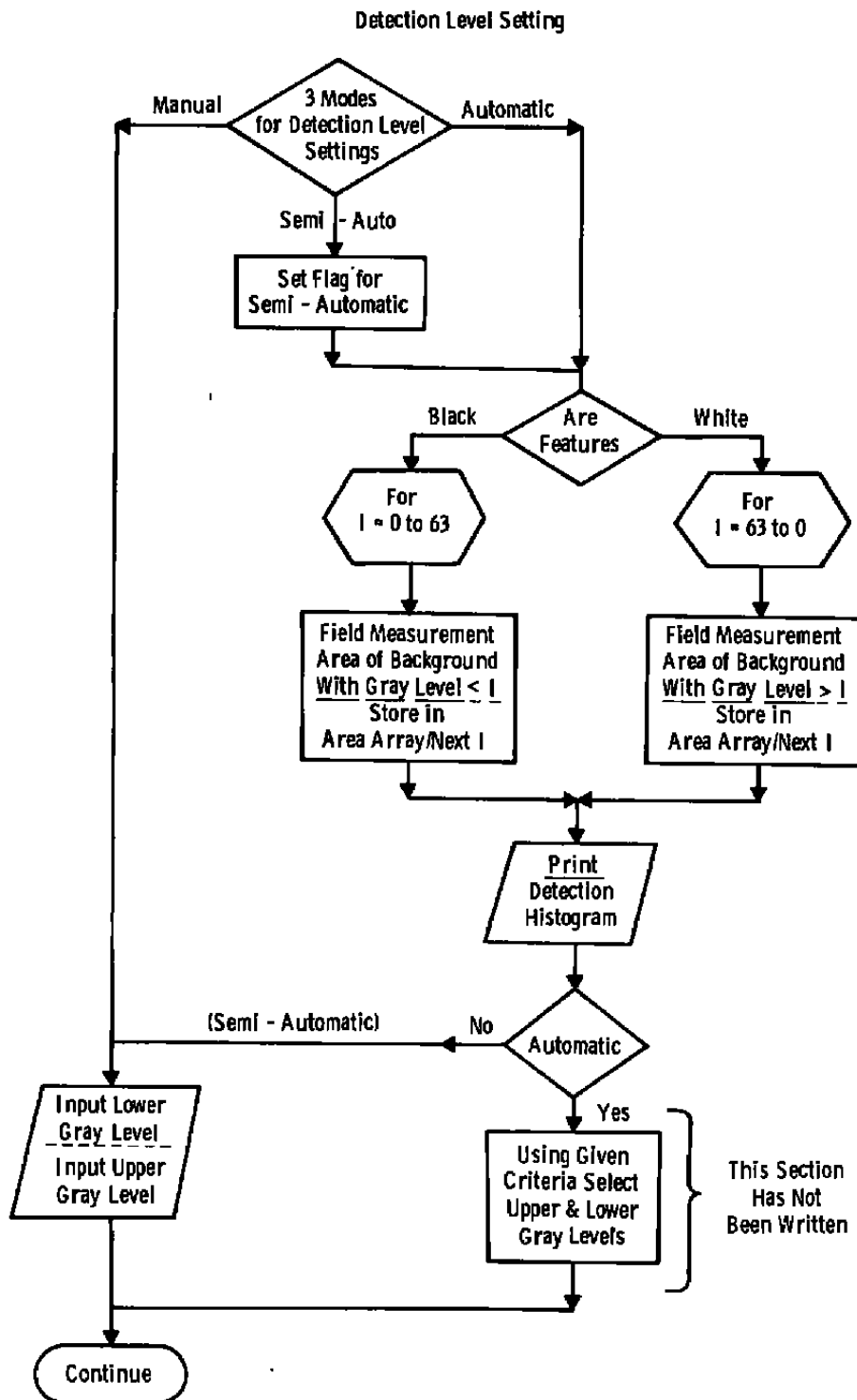


Figure 9. Flow chart of the detection level selection program.

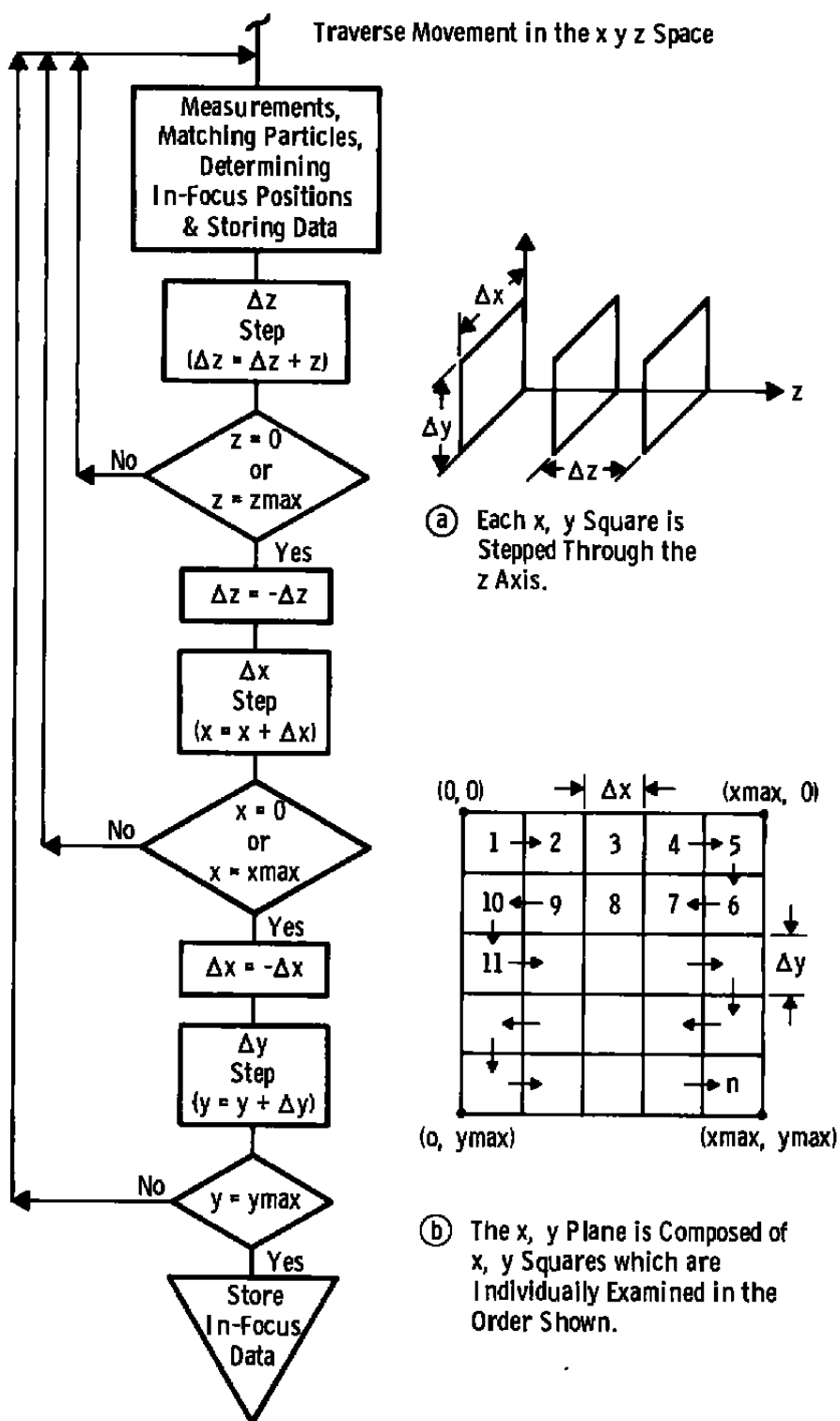
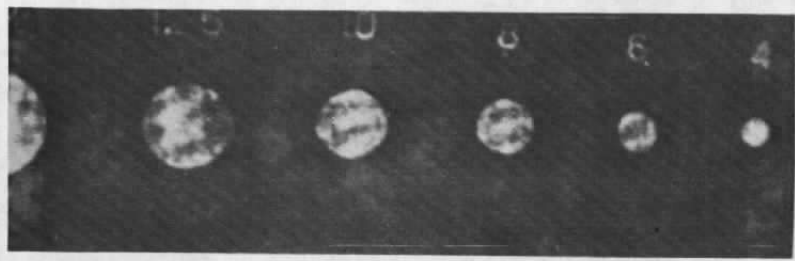
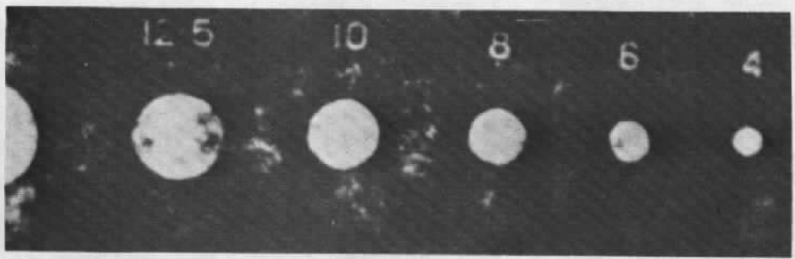


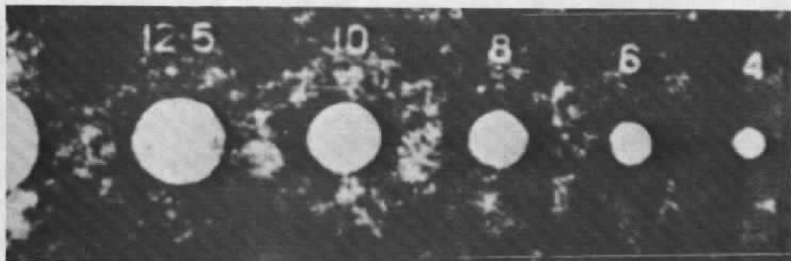
Figure 10. Flow chart of the traverse movement.



(a)



(b)

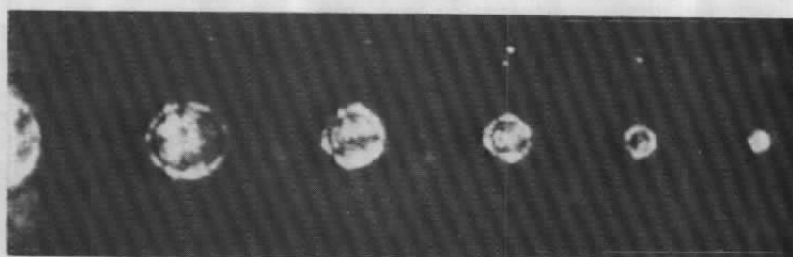


(c)

**Figure 11.** In-focus reconstructed particle images as observed at different detection levels.



a.  $\Delta z = 0$



b.  $\Delta z = 1,250 \mu\text{m}$



c.  $\Delta z = 2,500 \mu\text{m}$

Figure 12. Detected intensity levels within reconstructed particle images for out-of-focus distance  $\Delta z$ .

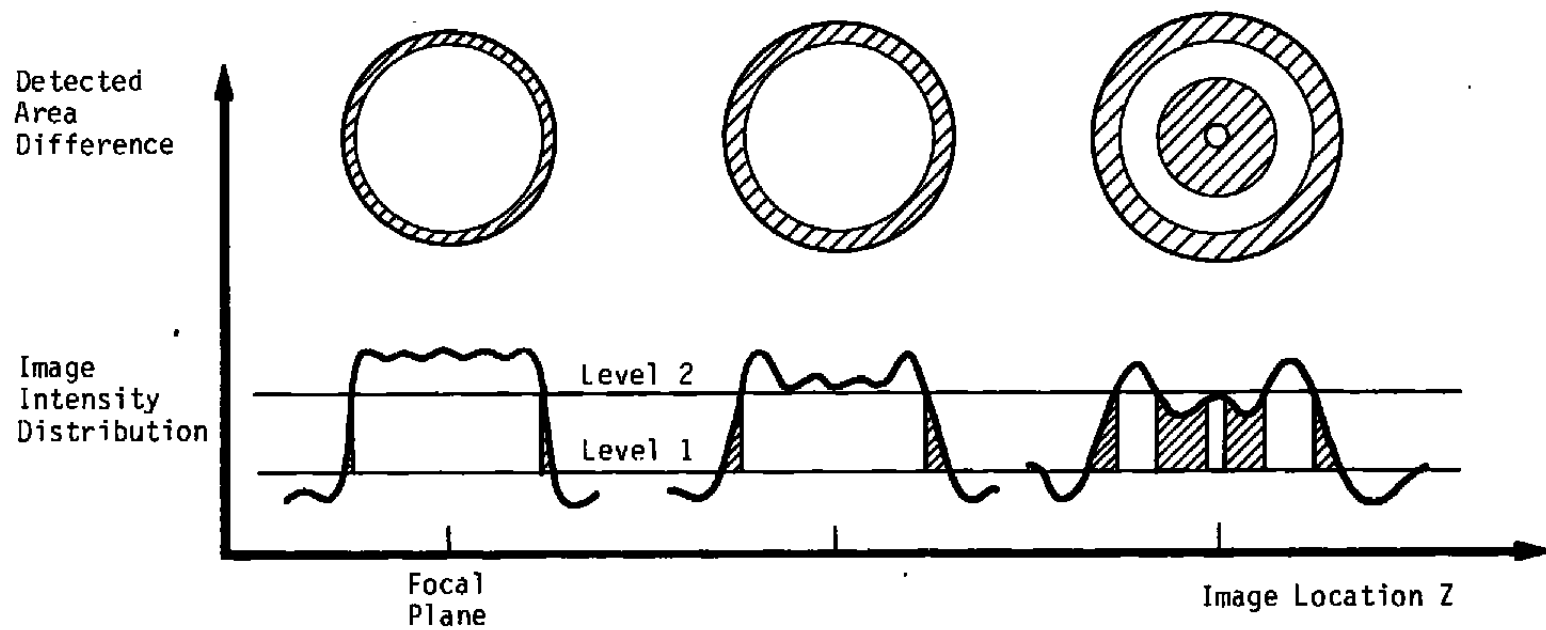


Figure 13. Principle of the area difference detection algorithm.

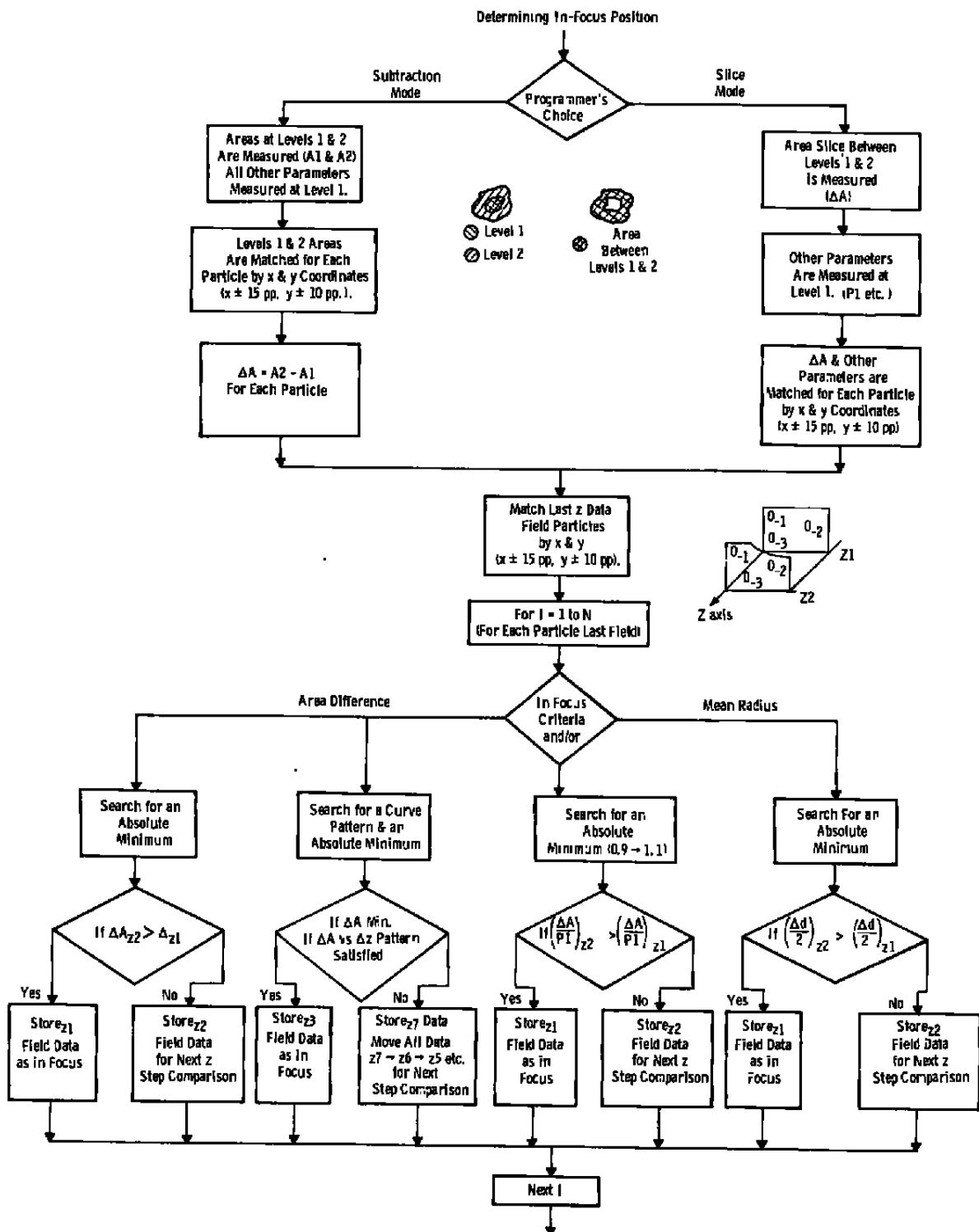


Figure 14. Flow chart of the focal detection algorithms.

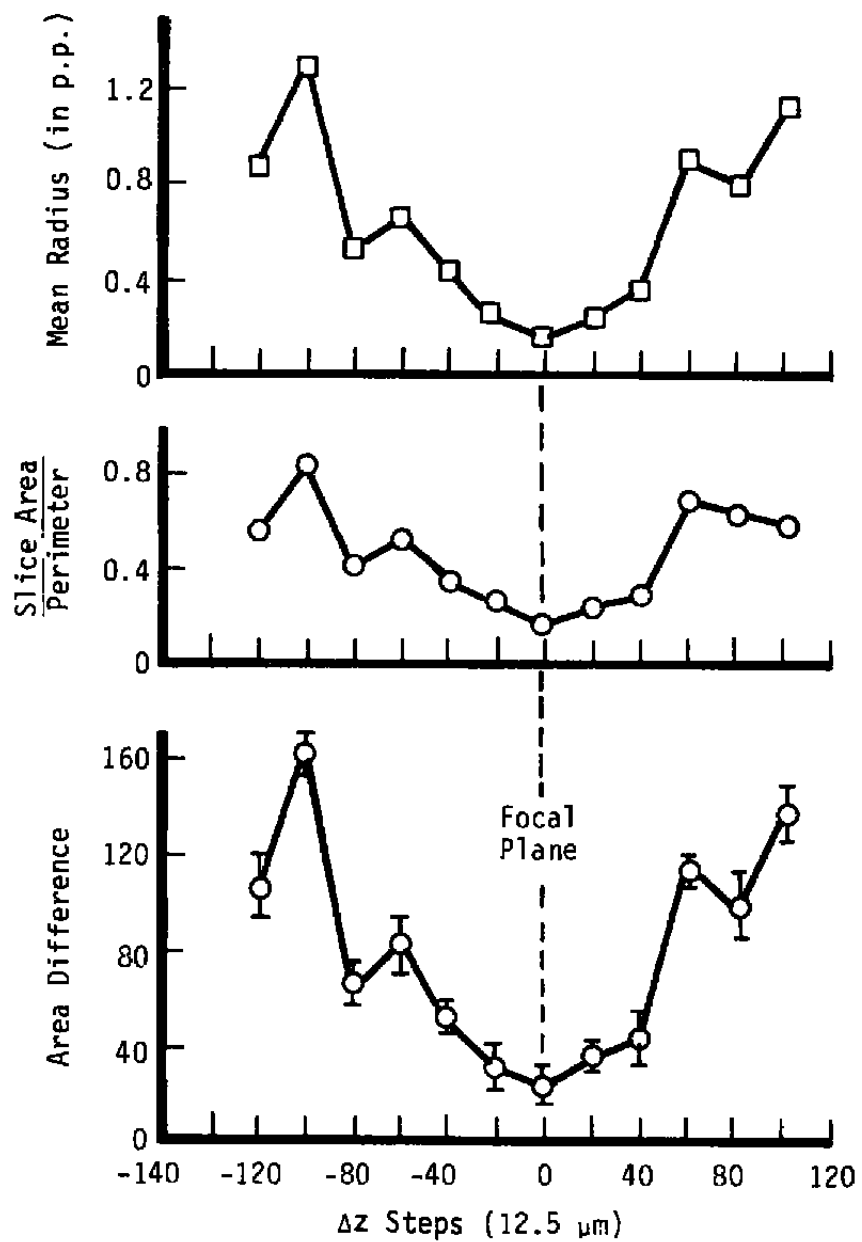


Figure 15. Focal detection of a particle image using the detection algorithms.

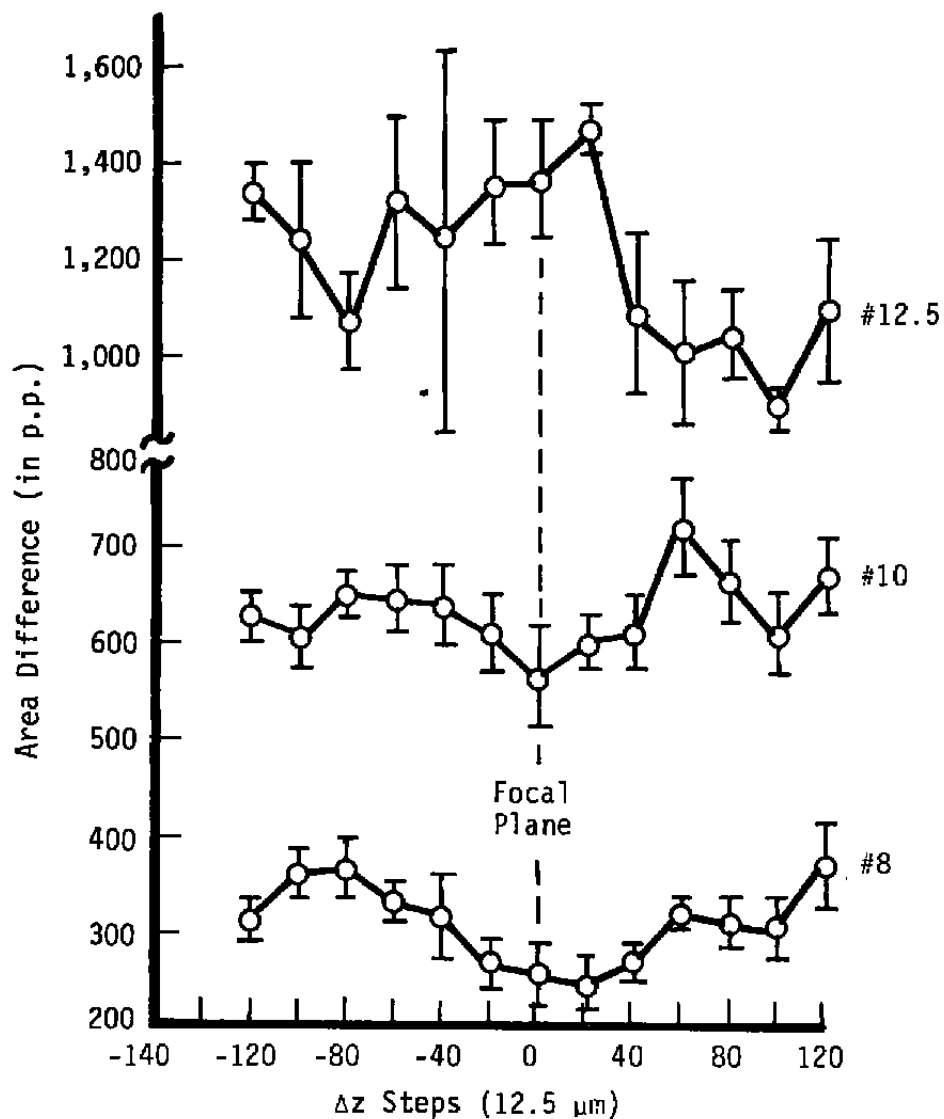


Figure 16. Focal detection by area difference of holographic particle images.

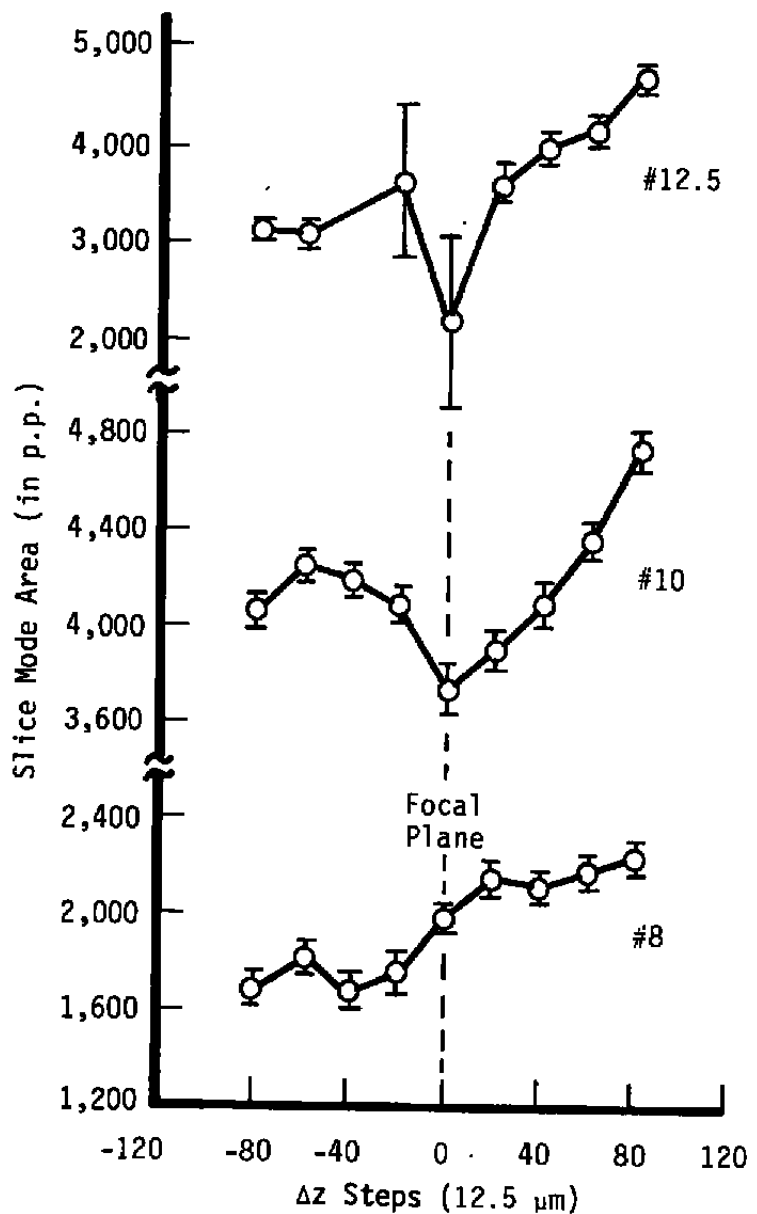


Figure 17. Focal detection by slice mode area of holographic particle images.

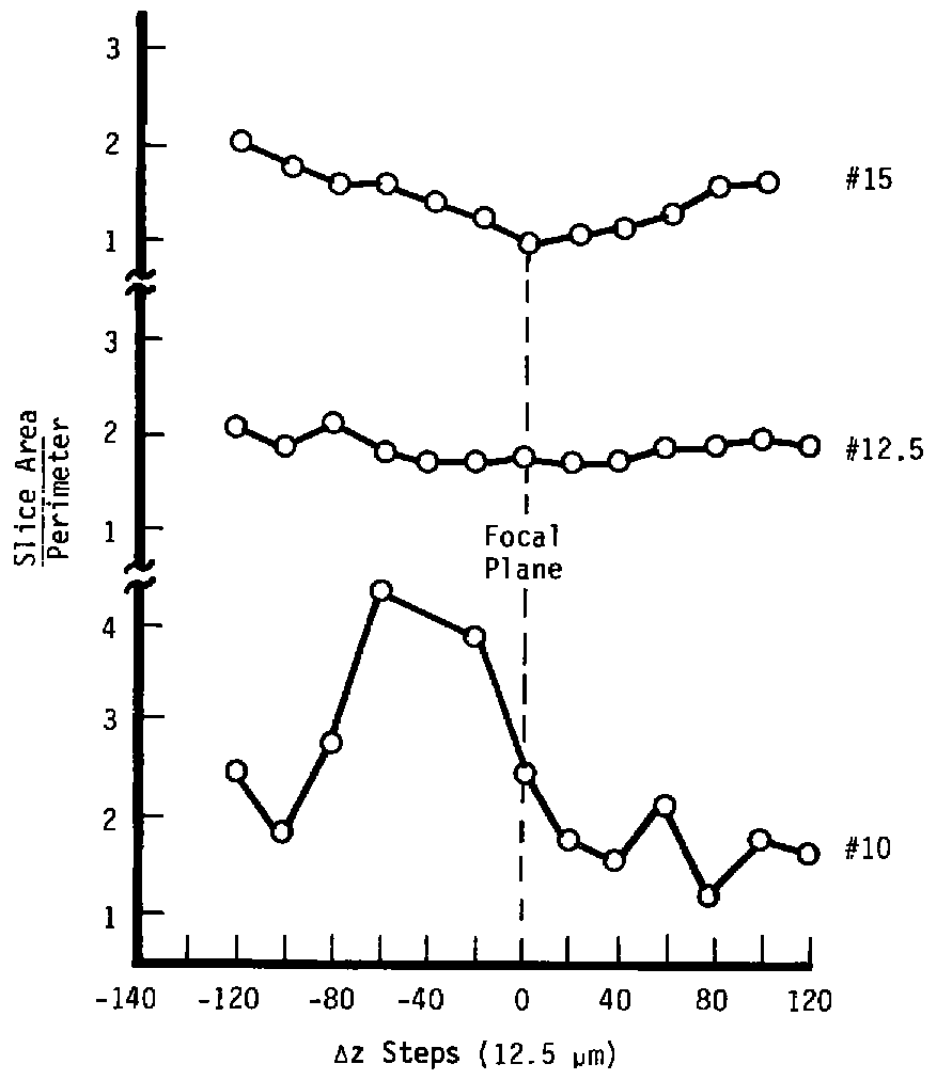


Figure 18. Focal detection by slice area divided by the perimeter of holographic particle images.



a.  $\Delta z = 0$



b.  $\Delta z = 1,250 \mu\text{m}$

Figure 19. Slice mode detection of reconstructed particle images for out-of-focus distance  $\Delta z$ .

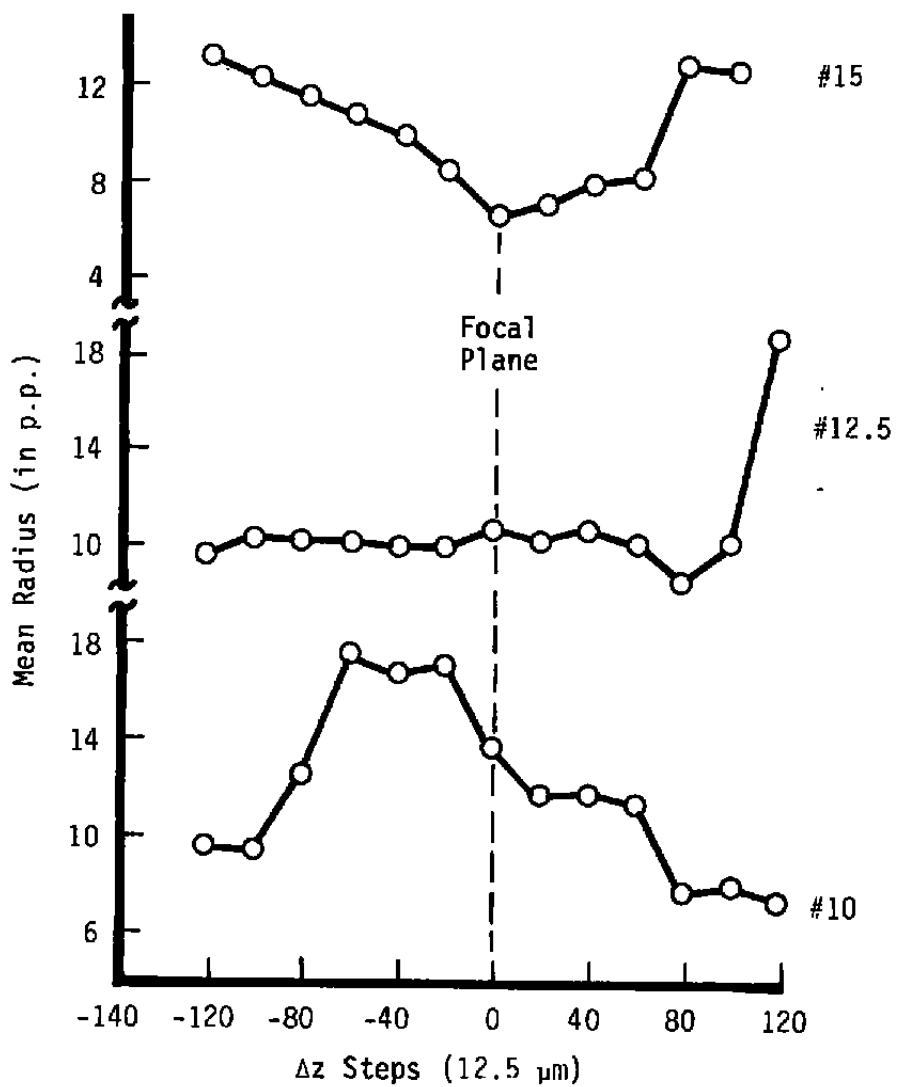


Figure 20. Focal detection by mean radius of holographic particle images.